CHEMISTRY OF MATERIALS
Article

Chem. Mater. **2009,** *21,* 2661–2667 2661
DOI:10.1021/cm900048e

Synthesis of Intermetallic PtZn Nanoparticles by Reaction of Pt Nanoparticles with Zn Vapor and Their Application as Fuel Cell Catalysts

Akira Miura, Hongsen Wang, Brian M. Leonard, Héctor D. Abruña, and Francis. J. DiSalvo*

Department of Chemistry and Chemical Biology, Baker Laboratory, Cornell University, Ithaca, New York 14853

Received January 7, 2009. Revised Manuscript Received May 11, 2009

Intermetallic PtZn nanoparticles with stable and high activities toward formic acid and methanol electrooxidation were synthesized by reaction of carbon-supported Pt nanoparticles with Zn vapor at 500 °C for 8 h under flowing nitrogen at atmospheric pressure. The resulting well-dispersed 3−15 nm diameter PtZn nanoparticles were tetragonal phase ($P4/mmm$: $a = 0.2842(1)$ nm, $c = 0.3488(3)$ nm) and their Pt:Zn ratio was approximately 1:1. Reactions using unsupported Pt nanoparticles (<5 nm domain size) produced aggregated masses consisting of 5−60 nm nanoparticles. The catalytic activities of supported PtZn nanoparticles toward formic acid and methanol electrooxidation were studied by differential electrochemical mass spectrometry (DEMS). The intermetallic PtZn nanoparticles exhibited higher currents for both formic acid and methanol oxidation than supported Pt nanoparticles with similar particle sizes, but the activity was not as high as that of PtPb. Finally, we established that vapor phase reactions of nano-Pt and M at temperatures sufficient to produce a vapor pressure of 1×10^{-4} atm for M are generally successful (M: Bi, Tl, and Pb).

1. Introduction

Polymer electrolyte membrane fuel cells (PEMFCs) have the potential to be a highly efficient energy conversion device for transportation and mobile applications.[1] PEMFCs usually use hydrogen as fuel; however, because of challenges in handling and storage of hydrogen especially for low power and mobile applications, methanol and formic acid have also been studied as potential fuels (so-called direct methanol and direct formic acid fuel cells). Pt metal or Pt-based compounds are key catalysts for electrooxidation of all of these fuels.[2,3] Pt−Ru alloy nanoparticles are the standard anode catalyst for PEMFC using methanol since it shows the highest catalytic activity and resistance to CO poisoning.[3−7] However, the overpotential on Pt−Ru is high (at least 0.3 V at reasonable power densities) and it has insufficient durability,[8] especially under nonoptimum conditions.[9] Recently, other Pt-based compounds, such as PtBi, PtPb, Pt_3Ti, Pt_3Sn, and Pt_3Ni, have been reported as potential catalysts for methanol or formic acid electrooxidation or oxygen electroreduction.[10−20] PtBi and PtPb are intermetallic compounds in which Pt and other metals, respectively, occupy unique crystallographic positions, whereas Pt−Ru and Pt_3Ni are alloys in which Pt and other metals statistically occupy the same crystallographic positions. Depending upon the mode and temperature of synthesis, Pt_3Sn and Pt_3Ti can form an ordered intermetallic or an alloy.

Because heterogeneous catalysis is a surface phenomenon, the composition and structure of the catalyst

*To whom correspondence should be addressed. E-mail: fjd3@cornell.edu.

(1) Lamy, C. L.; Leger, J.-M.; Srinivasan, S. Direct Methanol Fuel Cells: From a Twentieth Century Electrochemist's Dream to a Twenty-first Century Emerging Technology; Kluwer Academic/Plenum Publishers: New York, 2001; Vol. 34.
(2) Schmidt, T. J.; Gasteiger, H. A.; Behm, R. J. *J. Electrochem. Soc.* **1999**, *146*, 1296–1304.
(3) Costamagna, P.; Srinivisan, S. *J. Power Sources* **2001**, *102*, 242–252.
(4) Bockris, J.O'M.; Wroblowa, H. *J. Electroanal. Chem.* **1964**, *7*, 428–451.
(5) Petry, O. A.; Podlovchenko, B. I.; Frumkin, A. N.; Lal, H. *J. Electroanal. Chem.* **1965**, *10*, 253–269.
(6) Wang, H; Baltruschat, H. *J. Phys. Chem. C* **2007**, *111*, 7038–7048.
(7) Wang, H.; Wingender, C.; Baltruschat, H; Lopez, M.; Reetz, M. T. *J. Electroanal. Chem.* **2001**, *509*, 163–169.
(8) Taniguchi, A.; Akita, T.; Yasuda, K.; Miyazaki, Y. *J. Power Sources* **2004**, *130*, 42–49.
(9) Chen, W.; Sun, G.; Liang, Z.; Mao, Q.; Li, H.; Wang, G.; Xin, Q.; Chang, H.; Pak, C.; Seung, D. *J. Power Sources* **2006**, *160*, 933–939.
(10) Casado-Rivera, E.; Gál, Z.; Angelo, A. C. D.; Lind, C.; DiSalvo, F. J.; Abruña, H. D. *Chem. Phys. Chem.* **2003**, *4*, 193–199.
(11) Casado-Rivera, E.; Volpe, D. J.; Alden, L.; Lind, C.; Downie, C.; Vázquez-Alvarez, T.; Angelo, A. C. D.; DiSalvo, F. J.; Abruña, H. D. *J. Am. Chem. Soc.* **2004**, *126*, 4043–4049.
(12) Volpe, D. J.; Casado-Rivera, E.; Alden, L.; Lind, C.; Hagerdon, K.; Downie, C.; Korzeniewski, C.; DiSalvo, F. J.; Abruña, H. D. *J. Electrochem. Soc.* **2004**, *151*, A971–A977.
(13) Roychowdhury, C.; Matsumoto, F.; Mutolo, P. F.; Abruña, H. D.; DiSalvo, F. J. *Chem. Mater.* **2005**, *17*, 5871–5876.
(14) Roychowdhury, C.; Matsumoto, F.; Zeldovich, V.; Warren, S. C.; Mutolo, P. F.; Ballesteros, M.; Wiesner, U.; Abruña, H. D.; DiSalvo, F. J. *Chem. Mater.* **2006**, *18*, 3365–3372.
(15) Alden, L. R.; Han, D. K.; Matsumoto, F.; Abruña, H. D.; DiSalvo, F. J. *Chem. Mater.* **2006**, *18*, 5591–5596.
(16) Alden, L. R.; Roychowdhury, C.; Matsumoto, F.; Han, D. K.; Zeldovich, V.; Abruña, H. D.; DiSalvo, F. J. *Langmuir* **2006**, *22*, 10465–10471.
(17) Abe, H.; Matsumoto, F.; Alden, L. R.; Warren, S. C.; Abruña, H. D.; DiSalvo, F. J. *J. Am. Chem. Soc.* **2008**, *130*(16), 5452–5458.
(18) Matsumoto, F.; Roychowdhury, C.; DiSalvo, F. J.; Abruña, H. D. *J. Electrochem. Soc.* **2008**, *155*(2), B148–B154.
(19) Bauer, J. C.; Chen, X.; Liu, Q; Phan, T.-H.; Schaak, R. E. *J. Mater. Chem.* **2008**, *18*, 275–282.
(20) Stamenkovic, V. R.; Fowler, B.; Mun, B. S.; Wang, G.; Ross, P. N.; Lucas, C. A.; Markovic, N. M. *Science* **2008**, *315*, 493–497.

Published on Web 06/17/2009

surface are key factors in determining activity. However, the tools to unambiguously determine these surface properties, especially of in situ nanoparticles, are poorly developed. Nonetheless, it is clear that several factors will affect the surface composition and structure of any catalyst. The first factor is surface reaction upon exposure to air. Perhaps with the exception of Pt and Au, every elemental metal reacts with water or oxygen in air to form an oxide/hydroxide layer at the surface. This layer may be quite thin (a few nm) or quite thick (mm or more) and may react further, but more slowly, with lower concentration impurities in air to form carbonates, sulfates, etc. Sometimes this reaction layer can be removed or modified by in situ pretreatment, such as electrochemical cycling over an appropriate potential range. The second factor is especially important in electrochemical environments: leaching of the non-noble metal(s) from the surface or bulk of the catalyst. Leaching is the oxidative dissolution of metals from an alloy or intermetallic compound.[21] When leaching is carried out at or near room temperature, the process is kinetically controlled and the final compositions and structures are often far from equilibrium. Bulk leaching is dramatic, leading to gross mass loss and large increases in surface area. Surface leaching is less obvious and may affect only the top few atomic layers of the catalyst. Unless the electrochemical potentials are well below the standard reduction potentials of non-noble metals, at least some surface leaching is likely to occur. The free energies of formation of intermetallic compounds are much higher than those of alloys, leading to some stabilization against electrochemical leaching when compared to alloys containing that same non-noble metal. Although other factors, such as chemisorption of impurities such as carbon monoxide, sulfides, etc., may also be important in particular cases, the above two factors will always be in play, as we will see in this communication.

Combinatorial methods have been useful for high throughput screening.[22−25] T. He et al. have shown that Pt−Zn thin films exhibit high activities during oxygen electroreduction, but the Zn content decreases during the measurements because of leaching.[22,23] They do not report the crystal structure of the Pt−Zn film or its surface. A. Soda et al. has reported the surface morphology and composition of an electrochemically generated Pt−Zn alloy and tested its effectiveness toward oxygen reduction.[26] The Pt−Zn alloy is stable in acidic environment up to +1.2 V versus the reversible hydrogen electrode (RHE). Nonetheless, we believe that surface leaching of the Zn in Pt rich alloys in the top monolayer is likely. Nevertheless, these reports have not explored the catalytic activity and stability of a 1:1 intermetallic PtZn phase. Very recently, J. Gregoire et al. have showed that the stable intermetallic PtZn phase formed after leaching Zn from Zn-rich Pt−Zn alloys.[27] The activity of PtZn intermetallic for methanol oxidation was found to be competitive with Pt below 0.65 V and superior above 0.65 V. However, to the best of our knowledge, the catalytic activity of intermetallic PtZn nanoparticles for methanol and formic acid electrooxidation has not been reported.

Because Pt is a precious metal, Pt-based intermetallic compounds should be prepared as nanoparticles for practical applications in catalysis. Nanoparticles have been produced by mechanical methods[28] and by coreduction of precursors.[14−17] However, in the latter method, it is challenging to avoid chemisorption of species that may be present in the synthesis procedure (such as the solvent, anions, or neutral ligands from the metal containing reactants or reducing agents). Heating the synthesized nanoparticles in vacuum or inert gas may remove some of the impurities and organic compounds by evaporation, but may also cause particle growth.[17] PtZn nanoparticles have also been synthesized by heating Pt nanoparticles on a ZnO support in a reducing atmosphere,[29] but ZnO is not a suitable support for PEMFCs because of its low conductivity and solubility in acidic solutions.

In this report, we present the synthesis of intermetallic PtZn nanoparticles by reaction of Pt nanoparticles with Zn vapor under atmospheric pressure, as well as the activity of these PtZn nanoparticles toward formic acid and methanol electrooxidation. A related procedure of reacting nanoparticle metals (some of them are bound to supports), but carried out in organic solution, has also been recently reported for the synthesis of various intermetallic nanoparticles, such as Pt_3Sn, PtSn, PdZn, and $AuCuSn_2$[19,30−32] The present synthetic method has the following advantages: (1) No solvents, anions, or ligands are present in the process, so little to no contamination from those sources is expected, and (2) the carbon support significantly mitigates particle sintering. The disadvantage of the method is that rather few elemental metals are as or more volatile than Zn, so the method is not broadly applicable. Supported PtZn nanoparticles exhibited ca. 6 times higher current toward formic acid oxidation when compared to the supported Pt nanoparticles with similar particle sizes. Somewhat enhanced activity toward methanol oxidation was also observed.

(21) Sieradzki, K.; Corderman, R. R.; Shukla, K.; Newman, R. C. *Phil. Mag*. **1989**, *59*, 713–746.
(22) He, T.; Kreidler, E.; Xiong, L.; Ding, E. *J. Power Sources* **2007**, *25*, 87.
(23) He, T.; Kreidler, E; Xiong, L.; Luo, J.; Zhong, C. *J. Electrochem. Soc*. **2006**, *153*(9), A1637–A1643.
(24) Reddington, E.; Sapienza, A.; Gurau, B.; Viswanathan, R.; Sarangapani, S.; Smotkin, E. S.; Mallouk, T. E. *Science* **1998**, *280*, 1735–1737.
(25) Prochaska, M.; Jin, J.; Rochefort, D.; Zhuang, L.; DiSalvo, F. J.; VanDover, R. B.; Abruña, H. D. *Rev. Sci. Instrum*. **2006**, *77*, 054104.
(26) Soda, A.; Li, W.; Yang, Y.; Wong, P. C.; Gyenge, E.; Mitchell, K. A. R.; Bizzotto, D. *J. Phys. Chem. B* **2006**, *110*, 8715–8722.
(27) Gregoire, J. M.; Kostylev, M.; Tague, M. E.; Mutolo, P. F.; VanDover, R. B.; DiSalvo, F. J.; Abruña, H. D. *J. Electrochem. Soc*. **2009**, *156*(1), B160–A166.
(28) Honma, I.; Toda, T. *J. Electrochem. Soc*. **2003**, *150*(12), A1689–1692.
(29) Ammari, F.; Lamotte, J.; Touroude, R. *J. Catal*. **2004**, *211*, 32–42.
(30) Cable, R. E.; Schaak, R. E. *Chem. Mater*. **2007**, *19*, 4098–4104.
(31) Leonard, B. M.; Schaak, R. E. *J. Am. Chem. Soc*. **2006**, *128*, 11475–11482.
(32) Vasquez, Y.; Henkes, A. E.; Bauer, J. C.; Schaak, R. E. *J. Solid State Chem*. **2008**, *181*, 1509–1523.

2. Experimental Procedures

Chemicals. The following materials were used: Platinum(II) 2,4-pentanedionate ($Pt(acac)_2$) (Alfa Aesar), sodium metal (Aldrich), naphthalene (Fisher), Pt/Vulcan XC-72 (E-TEK, 50 wt % Pt), micrometer-sized Pt powder (50 mesh, ca. 1 μm grain size, no impurity detected by energy-dispersive X-ray analysis), Zn metal (Alfa Aesar, 99.999% purity), Ti powder (Alfa Aesar, 99.98%), Bi metal (Alfa Product, 99.999%), Pb metal (Cerac, 99.9999%), Tl metal (Alfa Aesar, 99.9%).

Synthesis of Unsupported Pt Nanoparticles. Platinum(II) 2,4-pentanedionate (222 mg: 0.565 mmol) was weighed out in a glovebox and dissolved in 5 mL of THF. This solution was sealed and brought out of the glovebox and then injected into the stirring sodium naphthalide solution, which was prepared from sodium metal (38 mg: 1.5 mmol) and naphthalene (205 mg: 1.5 mmol) in THF according to well-known literature methods.[33] The dark green solution immediately turned black. The Pt nanoparticle solution was stirred for 3 h, and the solvent was then pumped out of the flask by vacuum leaving the black Pt nanoparticles. The product was isolated by centrifugation (X2) after the addition of hexanes or 1:2 solution of hexane: methanol. The black precipitate was dried under a vacuum.

Conversion to PtZn Nanoparticles from Pt Nanoparticles. Unsupported Pt nanoparticles were preheated at 300 °C in N_2 flow for 8 h to remove any surface contamination by organic species and water. After preheating, the following procedures were performed in an argon atmosphere glovebox. The preheated Pt nanoparticles (19 mg) and a Zn chip (6 mg) were put in separate alumina boats, which were inserted into a silica glass crucible that was then capped by a graphite crucible. The molar ratio of Pt:Zn in the crucibles was 1:1. The Pt nanoparticles and Zn chip in the crucibles were set in a tube furnace without air exposure. Approximately 80 mg of Ti powder were placed just before the crucible to trap oxygen or water impurities. 99.995% pure nitrogen gas was flowed over the Ti and around the crucible at 500 °C for 8 h and then the furnace was turned off. Using an identical procedure, we also processed unsupported Pt micrometer-sized powder (19 mg) with a Zn chip (6 mg) to produce PtZn.

Pt nanoparticles supported on Vulcan (Pt/Vulcan) were also preheated in N_2 flow at 300 °C for 8 h. After preheating, a 15% weight loss occurred. Preheated Pt/Vulcan (10 mg) and Zn (2 mg) were heated in the same way as the unsupported Pt nanoparticles. The molar ratio of Pt:Zn in the crucibles was 1:1, assuming the amount of Pt did not decrease during preheating. To compare particle size and activity, we heated a sample of Pt/Vulcan with no Zn present.

Other Pt−M Reactions and Compounds. The preheated Pt/Vulcan (3 mg) was also heated with a Bi, Pb, or Tl chip (3−20 mg) at 500−730 °C for 8−32 h using the same procedure, in order to explore the possibility of synthesis Pt−Bi, Pt−Pb, and Pt−Tl intermetallics and the lower limit of the metal vapor pressure at which reasonable reaction rates are found for this method.

Characterization. Powder X-ray diffraction (pXRD; Scintag XDS 2000; Cu Kα radiation) was used for structural characterization. Images were taken with a scanning electron microscope (SEM; LEO-1550 field emission SEM) with energy-dispersive X-ray analysis (EDX), and also with an ultrahigh vacuum scanning transmission electron microscope (STEM; VG HB01UX UHV STEM) equipped with selected area electron diffraction (SAED). Isopropyl alcohol suspensions of the samples were dispersed on a Si wafer for SEM and on a commercial copper grid for TEM, respectively. Surface characterization was carried out by X-ray photoelectron spectroscopy (XPS; Surface Science Instrument SSX-100).

Electrochemical and DEMS Measurements. Catalyst suspensions of heated Pt/Vulcan and PtZn/Vulcan were prepared by mixing 8.0 mg (for Pt/Vulcan) or 9.6 mg (for PtZn/Vulcan) of catalyst, 3980 μL of water, 1000 μL of isopropanol, and 20 μL of 5% Nafion solution and sonicating for 10 min. Thin-film electrodes of either Pt/Vulcan and PtZn/Vulcan were prepared by pipetting and drying 20 μL of the catalyst suspension on a mirror-polished glassy carbon disk (Sigradur G from Hochtemperatur Werkstoffe GmbH, 6 mm in diameter). The above procedure leads to a noble metal loading of 67 $\mu g/cm^2$.

The differential electrochemical mass spectrometry (DEMS) apparatus has been described in detail in previous publications.[34] A dual thin-layer flow-through cell made of Kel-F was connected to the main chamber via an angle valve for DEMS experiments.[34,35] Electrolyte flow was driven by the hydrostatic pressure in the supply bottle (flow rate: 10 μL/s) to ensure a fast transport of the species formed at the electrode to the mass spectrometric compartment, where the volatile products were evaporated into the vacuum system of mass spectrometer (time constant, ca. 1 s).

Electrochemical experiments were carried out with an EG&G model 173 Potentiostat/Galvanostat, model 175 universal programmer, and a homemade data acquisition software (CV_EI400) combined with an NI-DAQ card. All potentials are referred to a RHE using 0.1 M H_2SO_4 solution.

3. Results and Discussion

Synthesis of PtZn and Pt−M Nanoparticles. After heating the unsupported Pt nanoparticles with a Zn chip in the crucible, 6 mg of weight loss of the Zn chip (ca. 95 wt %) and 5 mg of weight gain of Pt nanoparticles (ca. 25 wt %) were observed, implying Zn evaporation and subsequent reaction with the Pt nanoparticles. Figure 1 shows pXRD patterns of (a) unheated Pt nanoparticles, (b) PtZn nanoparticles synthesized from Pt nanoparticles and (c) micrometer-sized PtZn powder from Pt micrometer-sized powder. Unheated Pt nanoparticles give a broad peak at ca. 40° (Figure 1a), which is a feature of Pt nanoparticles with a domain size of < 5 nm. In fact, after it was heated at 500 °C for 8 h, only Pt peaks with a domain size of 22 nm were shown. Only PtZn peaks are observed after Pt nanoparticles were heated with Zn (Figure 1b). The structure of PtZn is the tetragonal AuCu structure, which is different from the face centered cubic structure of Pt. The lattice parameters of the PtZn were $a = 0.2841(2)$ nm, $c = 0.3483(4)$ nm, which are close to the reported values: $a = 0.2864$ nm, $c = 0.3510$ nm. The domain size of the PtZn nanoparticles was 18 nm,[36] indicating some growth in particle size. When micrometer-sized Pt particles were heated with Zn, both Pt and PtZn peaks are apparent (Figure 1c). The large size of the Pt micrometer-sized particles and an apparent

(33) Adam, W.; Arce, J. *J. Org. Chem.* **1972**, *37*, 507–508.
(34) Wang, H.; Alden, L.; DiSalvo, F. J.; Abruña, H. D. *Phys. Chem. Chem. Phys.* **2008**, *10*, 3739–3753.
(35) Wang, H.; Löffler, T.; Baltruschat, H. *J. Appl. Electrochem.* **2001**, *31*, 759–765.
(36) Warren, B. E. X-ray Diffraction, 1st ed.; Dover Pubulication Inc.: Mineola, NY, 1990.

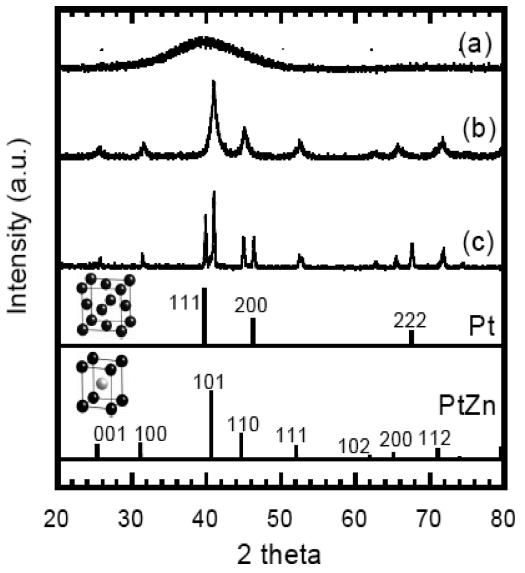

Figure 1. pXRD pattern of (a) unheated Pt nanoparticles, (b) PtZn nanoparticles synthesized by heating Pt nanoparticles with a Zn chip, and (c) PtZn micrometer-sized particles synthesized by heating Pt micrometer-sized particles with a Zn chip. Pt (JCPDS: 04−001−0112) and PtZn (JCPDS: 01−072−3027) are shown.

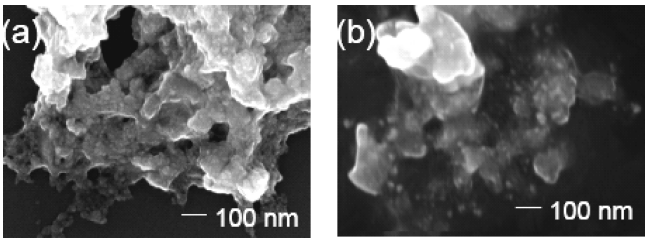

Figure 2. SEM images of (a) unheated Pt nanoparticles and (b) PtZn nanoparticles synthesized by heating Pt nanoparticles with a Zn chip.

slow diffusion rate of Zn in Pt particles prevent complete conversion to PtZn.

Figure 2 shows SEM images of unheated and unsupported Pt nanoparticles and unsupported PtZn nanoparticles. Pt nanoparticles form submicrometer-sized aggregates with rough surfaces (Figure 2a). The rough surface probably arises from the small domain size of the Pt nanoparticles, as suggested by the broad diffraction peak (Figure 1a). PtZn nanoparticles are also aggregated and have domain sizes of approximately 10−20 nm (Figure 2b). Figure 3 presents STEM images of the PtZn nanoparticles, showing the separated and aggregated nanoparticles were typically 5−20 nm in size (Figure 3a and b), but a few larger crystals around 60 nm were also observed. The light gray "halo" covering the nanoparticles is likely due to sodium oxide/hydroxide, zinc oxide/hydroxide and/or organic compounds, which were detected by XPS measurement (see Figure S1 in the Supporting Information). These compounds are residual byproducts of the synthesis of PtZn nanoparticles, which may result from exposure to air prior to characterization. The symmetric spot pattern of the SAED indicates that the nanoparticles are crystalline (Figure 3 c and d). Semiquantitative analysis via EDX showed that the Pt:Zn ratio was 44(2):56(2), which is 1:1 within experimental

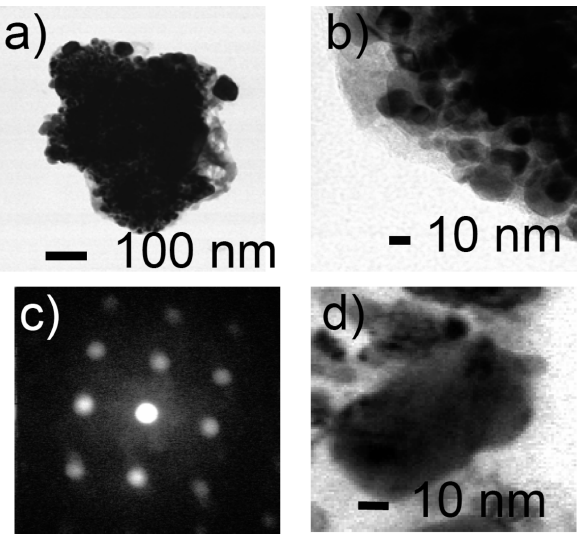

Figure 3. STEM and SAED images of PtZn nanoparticles: (a) an aggregate of nanoparticles, (b) edges of aggregated nanoparticles, (c) SEAD pattern with (d) the corresponding nanoparticle.

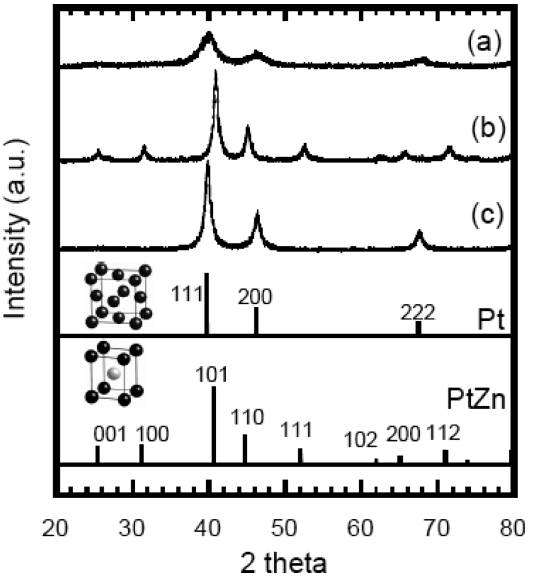

Figure 4. pXRD pattern of (a) unheated Pt/Vulcan, (b) PtZn/Vulcan synthesized by heating Pt/Vulcan with a Zn chip, (c) Pt/Vulcan heated without a Zn chip. Pt (JCPDS: 04−001−0112) and PtZn (JCPDS: 01−072−3027) are shown.

error for this semiquantitative measurement (see Figure S2 in the Supporting Information).

PtZn/Vulcan was also synthesized using Pt/Vulcan as a starting material. Two mg of weight gain of the Pt/Vulcan (ca. 16 wt. %) and 2 mg weight loss of the Zn chip (ca. 100 wt %) were observed after the heating of the Pt/Vulcan with the Zn chip. Figure 4a shows the pXRD pattern of the unheated Pt/Vulcan, which yields Pt peaks with a domain size of ca. 3 nm[36] and a weak and broad Vulcan peak around 26° (see Figure S3 in the Supporting Information). The Pt/Vulcan heated with Zn shows a tetragonal PtZn phase (Figure 4b), whose lattice parameters were almost the same as that of the unsupported ones ($a = 0.2842(1)$ nm and $c = 0.3488(3)$ nm). The domain size of the supported PtZn was 15 nm[36] and while domain

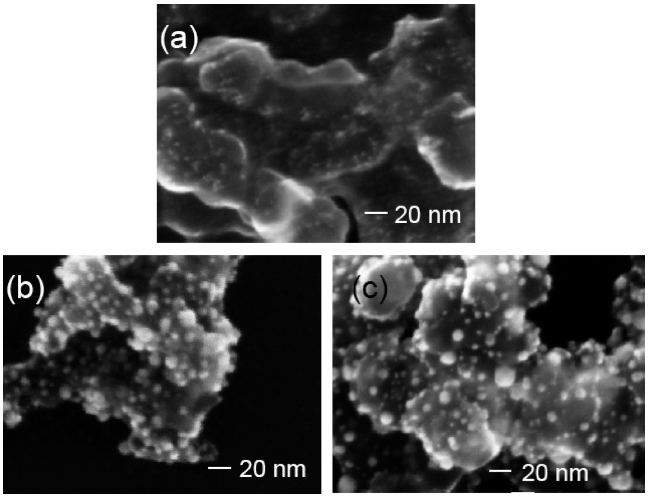

Figure 5. SEM images of (a) unheated Pt/Vulcan, (b) PtZn/Vulcan synthesized by heating Pt/Vulcan with a Zn chip, (c) Pt/Vulcan heated without a Zn chip.

growth from 3 to 15 nm is evident, it was moderate when compared with the unsupported PtZn particles (domain size: 18 nm). The Pt/Vulcan heated in the absence of Zn exhibited Pt peaks with the same domain size as that of PtZn/Vulcan (15 nm[36]) (Figure 4c).

Figure 5 shows SEM images of (a) unheated Pt/Vulcan, (b) PtZn/Vulcan, and (c) heated Pt/Vulcan. The unheated Pt/Vulcan exhibits Pt nanoparticles of 3−5 nm on the carbon support (Figure 5a). The PtZn/Vulcan showed nanoparticles ranging from 3 to 15 nm, indicating particle growth (Figure 5b). However, the aggregation is clearly suppressed when compared to the unsupported PtZn nanoparticles. EDX spectra of PtZn/Vulcan showed a Pt:Zn ratio of 52(7)%:48(2)% (see Figure S4 in the Supporting Information), which is close to 1:1. XPS indicated their surface is Zn-rich and covered with negligible Na compounds, as expected since Na is not included in the synthesis (see Figure S5 in the Supporting Information). The Pt/Vulcan heated at 500 °C without Zn contains nanoparticles from 3 to 15 nm (Figure 5c), which is not significantly different from those found in PtZn/Vulcan. The maximum size of both the heated Pt and PtZn nanoparticles is 15 nm, consistent with the domain size derived from the *p*XRD data.

We believe that the conversion from Pt to PtZn proceeds in three steps: (1) generation of Zn vapor, (2) adsorption and desorption of Zn atoms to/from the surface of Pt nanoparticles, and (3) diffusion of Zn metal into the bulk of Pt nanoparticles. After the zinc chip was heated at 500 °C, nearly all of the Zn evaporated. The Zn vapor pressure is estimated to be ca. 2×10^{-3} atm,[37] which should be high enough for rapid evaporation. Following evaporation, adsorption of Zn atoms on the Pt surface should occur. Although we do not obtain evidence to support the desorption of Zn atoms from the Pt surface, the repeated adsorption and desorption of Zn may lead to nanoparticles of a uniform composition.

(37) Lide, D. R. CRC Handbook of Chemistry and Physics, 73rd ed.; CRC Press: Boca Raton, FL, 1992; pp 5−81.

Table 1. Reaction between Preheated Pt/Vulcan with Bi, Pb, or Tl Metal[1]

metal	temp. and time	vapor pressure (atm)	phase
Bi	580 °C/8 h	7×10^{-638}	Pt
Bi	630 °C/8 h	3×10^{-538}	U, $Pt^{(m)}$
Bi	705 °C/8 h	1×10^{-438}	$PtBi_2$, $U^{(w)}$
Pb	500 °C/8 h	2×10^{-837}	Pt
Pb	700 °C/8 h	9×10^{-637}	Pt
Pb	770 °C/32 h	4×10^{-537}	PtPb, Pt, $U^{(w)}$
Tl	630 °C/8 h	2×10^{-537}	$PtTl_2$, $Pt^{(w)}$
Tl	730 °C/8 h	2×10^{-437}	$PtTl_2$, $Pt^{(m)}$

[a] Phases were identified using the following JCPDS data files: 04-001-0112 (Pt), 00-009-0263 ($PtBi_2$), 04-001-2727 (PtPb), and 00-025-0613 ($PtTl_2$). "U" is unidentified phase. Subscript (w) and (m) indicate weak and minor signals, respectively.

While the diffusion rate of Zn in Pt at 500 °C was apparently high enough for the full conversion of Pt nanoparticles, it was not sufficient for full conversion of the micrometer-sized Pt particle. The high surface area and the small diffusion distance of Pt nanoparticles enable this complete conversion.

Synthesis of other intermetallic compounds ($PtBi_2$, PtPb, and $PtTl_2$) was attempted via a similar strategy using different metals and heating protocols, as shown in Table 1. This method may be useful for the synthesis of other intermetallic compounds when the vapor pressure of metals is at or above 1×10^{-5} atm at the synthesis temperature. For the PtZn synthesis, however, neither weight loss of a Zn chip nor PtZn phase were observed at a synthesis temperature of 450 °C, even though the vapor pressure is estimated to be 5×10^{-4} atm.[37] Interestingly, it did not appear that the Zn chip melted at 450 °C, though this temperature is above the melting point of Zn (419.58 °C). This may be due to the cooling effect of the flowing nitrogen gas through the silica tube. Perhaps Zn evaporation was also kinetically hindered due to a thin oxide layer on the zinc chip, which could be produced by oxygen containing impurities in the glovebox or in the 99.995% pure flowing nitrogen. At 500 °C, it was very apparent that the Zn melted and evaporated, perhaps disrupting any oxide layer on the surface. The correlation between the vapor pressure and synthesized phases (Table 1) and the unsuccessful synthesis of PtZn at 450 °C indicate that the rate-limiting factor of this synthesis procedure is the evaporation of the second metal.

Electrocatalytic Activity of PtZn Nanoparticles. Figure 6 presents a cyclic voltammogram of the PtZn/Vulcan in 0.1 M sulfuric acid, which is compared with the heated Pt/Vulcan with a same domain size, similar morphology and same loading amount of Pt. The heated Pt/Vulcan electrode showed two pairs of hydrogen adsorption/desorption peaks between 0.05 and 0.35 V in the cyclic voltammograms, typical characteristics of polycrystalline platinum. In contrast, the PtZn/Vulcan exhibited symmetric hydrogen adsorption/desorption currents in the low potential region without the clear peaks. One would anticipate that PtZn/Vulcan and Pt/Vulcan have quite different surface properties.

Figure 7 shows (a) the cyclic voltammogram of PtZn/Vulcan in 0.5 M HCOOH + 0.1 M H_2SO_4 solution and (b) corresponding mass spectrometric cyclic voltammogram

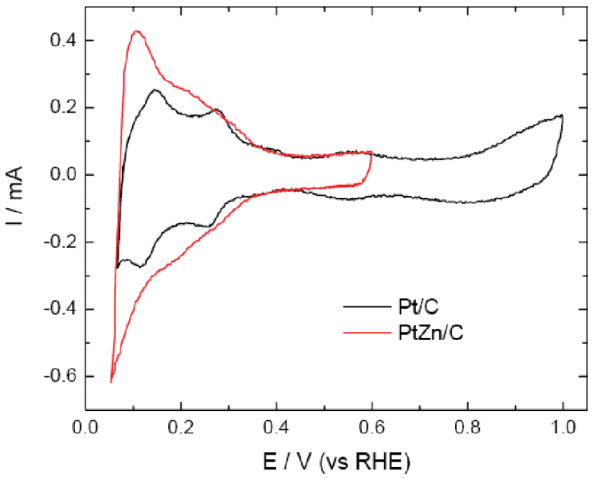

Figure 6. Cyclic voltammograms obtained on PtZn/Vulcan and heated Pt/Vulcan in 0.1 M sulfuric acid solution. Scan rate: 50 mV/s.

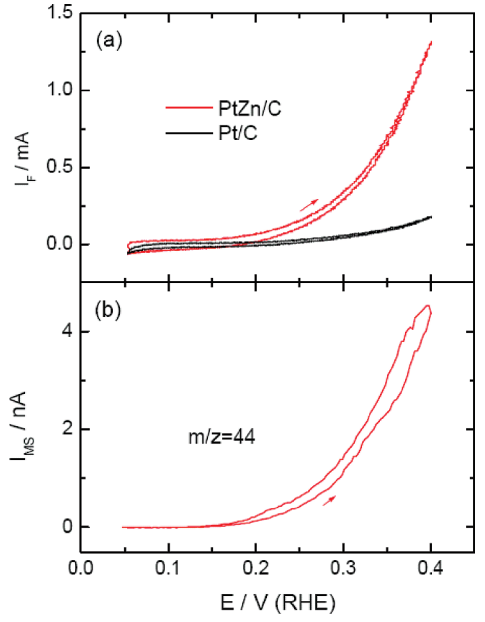

Figure 7. Simultaneously recorded (a) cyclic voltammograms and (b) corresponding mass spectrometric cyclic voltammogram of CO_2 at m/z = 44 for formic acid oxidation on PtZn/Vulcan and heated Pt/Vulcan in 0.5 M HCOOH + 0.1 M H_2SO_4 solution. Scan rate: 10 mV/s. The noble metal loading: 19 μg, i.e., 67 μg/cm^2.

of CO_2 at m/z = 44. For comparison, a cyclic voltammogram of the heated Pt/Vulcan is also shown. A slightly negative shift (ca. 50 mV) in the onset potential is observed for PtZn/Vulcan compared to Pt/Vulcan, while the oxidation current is significantly enhanced. For example, at +0.4 V, the oxidation current increases by ca. 6 times. To confirm that the oxidation current originates from formic acid oxidation, not from Zn oxidation, we also monitored CO_2 formation by DEMS (Figure 7b). The mass spectrometric current at m/z = 44 exactly follows the Faradaic current of formic acid oxidation, thus ruling out rapid Zn oxidation over the studied potential region. Pt/Vulcan exhibited a low activity toward formic acid oxidation due to CO poisoning, which

(38) Granovskaya, A.; Lyubimov, A. *Zh. Fiz. Khim.* **1948**, *22*, 103–106.

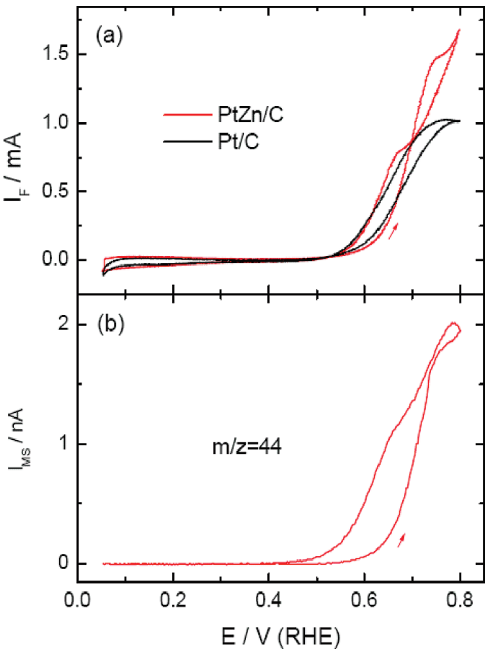

Figure 8. Simultaneously recorded (a) cyclic voltammograms and (b) corresponding mass spectrometric cyclic voltammogram of CO_2 at m/z = 44 for methanol oxidation on PtZn/Vulcan and heated Pt/Vulcan in 0.2 M CH_3OH + 0.1 M H_2SO_4 solution. Scan rate: 10 mV/s. The noble metal loading: 19 μg, i.e., 67 μg/cm^2.

originates from HCOOH decomposition at the defect, vertices, and step sites of Pt nanoparticles. At the PtZn/Vulcan nanoparticle surface, HCOOH decomposition to form adsorbed CO could be suppressed because of "third body" effects.[39] Formation of intermetallic PtZn reduces the number of Pt ensembles that are required to form adsorbed CO and thus inhibits HCOOH decomposition to form adsorbed CO.

The electrooxidation activities of methanol at PtZn/Vulcan and heated Pt/Vulcan are compared in Figure 8. Although PtZn/Vulcan exhibits the same onset potential (around 0.5 V) as heated Pt/Vulcan toward methanol oxidation, it has a somewhat higher oxidation current above +0.65 V, in agreement with the activities found in porous intermetallic PtZn films.[27] The formation of CO_2 detected by DEMS follows the oxidation current (Figure 8b), indicating that the current originates from methanol oxidation. The current efficiency for CO_2 formation was calculated to be ca. 97%, which is much higher than that of Pt/Vulcan (60%). This means that the PtZn/Vulcan can enhance the complete oxidation of methanol to CO_2. We did not see any significant changes in the cyclic voltammograms of PtZn/Vulcan during the scanning cycles between 0.05 and 0.80 V. However, when scanning between 0.05 and 1.00 V, the oxidation current decreased in the first several cycles and then increased with further cycling. Thus, it appears that the PtZn/Vulcan catalyst is stable at the potentials up to +0.80 V, but is unstable, likely because of Zn leaching out, in the range of 0.80−1.00 V.

(39) Angerstein-Kozlowska, H.; MacDougall, B.; Conway, B. E. *J. Electrochem. Soc.* **1973**, *20*, 756–766.

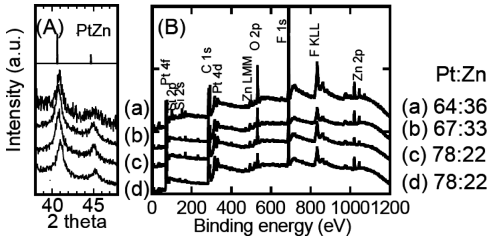

Figure 9. (A) pXRD and (B) XPS of PtZn-Vulcan-Nafion electrodes on Si wafers (a) before electrochemical test, (b) after 10 cycles at 10 mV/s between 0.05 and 0.6 V in 0.1 M H_2SO_4 solution, (c) after 10 cycles at 10 mV/s between 0.05 and 0.4 V in 0.5 M HCOOH + 0.1 M H_2SO_4 solution, (d) after 10 cycles at 10 mV/s between 0.05 and 0.8 V in 0.2 M CH_3OH + 0.1 M H_2SO_4 solution. Pt:Zn ratios determined by XPS are shown.

The stability of PtZn nanoparticles below the potential of 0.80 V was also examined by both pXRD and XPS of the PtZn-Vulcan-Nafion electrodes on electrically conductive Si wafers before and after the cyclic voltammograms (Figure 9). pXRD showed two characteristic peaks of PtZn before and after the electrochemical tests in sulfuric acid, formic acid or methanol solution (Figure 9A). XPS data indicate that the surfaces of PtZn nanoparticles in all the thin-film electrodes were Pt-rich, implying the leaching of Zn from Zn-rich surface (Figure 9B). The Pt:Zn ratio did not significantly change after voltage was applied only in sulfuric acid, but the amount of Zn decreased further (but not to zero) after the electrooxidation of formic acid and methanol.

The standard reduction potential (E^0) can be used as a measure of the stability of metals in electrochemical environments. In the case of Pt and Zn, the E^0 values are 1.18 and −0.76 V, respectively.[40] The formation energy of PtZn is calculated to be −108 kJ/mol,[41] which according to $\Delta E = -\Delta G^0_f/zF$ would shift the E^0 to more positive potential by 0.560 V. Because the E^0 value of Zn in PtZn would still be negative potential of −0.20 V, Zn leaching from bulk PtZn bulk would be thermodynamically favored. XPS experimentally supported the Zn leaching. However, the electrochemical experiments exhibited a steady activity toward formic acid and methanol oxidation at potentials below 0.8 V. In addition, the PtZn phase was observed after the electrooxidation by pXRD. These results suggest a kinetic stabilization of PtZn nanoparticles after the partial leaching of Zn from their surface. The PtZn nanoparticles could be stabilized by a Pt (or Pt-rich) skin/skeleton on their surfaces,[27] as has been reported for surfaces of bulk Pt−Co, Pt−Ni and Pt−Fe alloys.[42,43]

4. Conclusions

Intermetallic PtZn nanoparticles were successfully synthesized via vapor−solid reaction between Pt nanoparticles and Zn vapor at 500 °C for 8 h under flowing nitrogen at atmospheric pressure. The synthesized PtZn nanoparticles exhibited a tetragonal phase, and contained Pt and Zn in about a 1:1 ratio. The use of a high-surface-area carbon support (Vulcan XC-72) was allowed for the synthesis of well-dispersed 3−15 nm diameter PtZn nanoparticles. This simple conversion method could be applied to various other alloy/intermetallic nanoparticles containing metals that reach vapor pressures in the range of 1×10^{-4} to 1×10^{-5} atm at moderate temperatures.

The synthesized PtZn nanoparticles supported on carbon were stable during electrooxidation of formic acid and methanol up to +0.8 V (RHE), possibly because of the formation of a Pt skin covering the intermetallic nanoparticles. The PtZn intermetallic phase exhibited enhanced electrooxidation currents, especially for formic acid, when compared to Pt. However, the onset potential of intermetallic PtZn nanoparticles toward formic acid and methanol electrooxidation were higher than those of previous reported PtPb and PtRu,[3−7,13−15] so we will continue to explore binary and ternary materials, which could surpass the electrocatalytic activities of those materials.

Acknowledgment. This work was supported by DOE Grant DE-FG02-87ER45298. A.M. acknowledges Ambassadorial Scholarships from Rotary Foundation. A.M. thanks Malcolm Thomas and Jonathan Shu at the Cornell Center for Materials Research for help with the SEM, STEM, and XPS data collection.

Supporting Information Available: This material is available free of charge via the Internet at http://pubs.acs.org.

(40) Lide, D. R. CRC Handbook of Chemistry and Physics, 73rd ed.; CRC Press: Boca Raton, FL, 1992; pp 8−20 and 22.
(41) Miedema, A. R.; Dechâtel, de Boer, F. R. *Physica B* **1980**, *100*, 1–28.
(42) Stamenkovic, V. R.; Mun, B. S.; Mayrhofer, K. J. J.; Ross, P. N.; Markovic, N. M. *J. Am. Chem. Soc.* **2006**, *128*, 8813–8819.
(43) Toda, T.; Igarashi, H.; Uchida, H.; Watanabe, M. *J. Electrochem. Soc.* **1999**, *146*, 3750–3756.